Perovskites

Deutsche Ausgabe: DOI: 10.1002/ange.201608160
Internationale Ausgabe: DOI: 10.1002/anie.201608160

Lead-Free, Blue Emitting Bismuth Halide Perovskite Quantum Dots

Meiying Leng[+], Zhengwu Chen[+], Ying Yang[+], Zha Li, Kai Zeng, Kanghua Li, Guangda Niu, Yisu He, Qingchao Zhou, and Jiang Tang**

Abstract: *Lead halide perovskite quantum dots (QDs) are promising candidates for future lighting applications, due to their high quantum yield, narrow full width at half maximum (FWHM), and wide color gamut. However, the toxicity of lead represents a potential obstacle to their utilization. Although tin(II) has been used to replace lead in films and QDs, the high intrinsic defect density and oxidation vulnerability typically leads to unsatisfactory material properties. Bismuth, with much lower toxicity than lead, is promising to constitute lead-free perovskite materials because Bi^{3+} is isoelectronic to Pb^{2+} and more stable than Sn^{2+}. Herein we report, for the first time, the synthesis and optical characterization of $MA_3Bi_2Br_9$ perovskite QDs with photoluminescence quantum yield (PLQY) up to 12 %, which is much higher than Sn-based perovskite nanocrystals. Furthermore, the photoluminescence (PL) peaks of $MA_3Bi_2X_9$ QDs could be easily tuned from 360 to 540 nm through anion exchange.*

The last two decades have witnessed the successful development of quantum dots (QDs) with unique photonic and electronic properties. Among these materials, the newly emerged lead halide perovskite ($APbX_3$, $A = CH_3NH_3$ (MA), Cs; X = Cl, Br, I) QDs have drawn extensive attention.[1] Besides low cost and facile synthesis process, the band gaps of perovskite QDs can be conveniently tuned through controlling the halide compositions or utilizing quantum size effects, covering the whole visible spectrum from 400–800 nm. In addition, compared with traditional Cd-based QDs[2] (CdSe, CdS, etc.), lead halide perovskite QDs show comparable PLQY (≈90 %), narrower FWHM (12–25 nm) and wider color gamut (≈150 % NTSC).[3] As for optoelectronic applications, lead-based perovskite QDs have shown decent performance.[4] However, the toxicity of lead can be a great hindrance to applications in daily life.

Recently, lead-free perovskite materials have been studied for photovoltaic applications.[5] For perovskite QDs, to our best knowledge, only Böhm and co-workers reported the replacement of lead with non-toxic tin in spatially confined nanocrystals, producing $CsSnX_3$ nanocrystals.[6] Unfortunately, a rather low PLQY of 0.14 % was observed, much lower than Pb-based analogues, which was found to be related to the intrinsic defect sites and oxidation process from Sn^{II} to Sn^{IV}, commonly observed in Sn-based perovskites. Bismuth, with much lower toxicity than lead (according to materials safety data sheet), is promising to constitute perovskite materials because Bi^{3+} is isoelectronic with Pb^{2+} and more stable than Sn^{2+}.[7] However, there is no report about nanostructural Bi-based perovskites yet.

Here we report, for the first time, the synthesis and optical characterization of $MA_3Bi_2X_9$ (X = Cl, Br, I) perovskite QDs. $MA_3Bi_2Br_9$ perovskite QDs were synthesized by a collaborative solvent ligand-assisted re-precipitation (Co-LARP) method.[8] The PL peaks could be tuned from 360 to 540 nm through halide composition control. For $MA_3Bi_2Br_9$ QDs with an average diameter of 3.05 nm, we observed an emission peak at 430 nm and a PLQY as high as ca. 12 %. It should be noted that the value was even comparable to all-inorganic Pb-based QDs with similar emission peaks (e.g. $CsPbCl_3$ QDs, emission peak: 405 nm, PLQY: 10 %). In addition, it was also found that the alcohol stability of $MA_3Bi_2Br_9$ QDs was much better than that of $MAPbBr_3$ analogues.

Firstly, we prepared a $MA_3Bi_2Br_9$ single crystal, with a size of 1.97 mm × 2.01 mm × 0.46 mm, to obtain structural and optical information (Figure 1 a), due to its free-of-grain boundaries and less defects. X-ray diffraction (XRD) measurements (Figure 1 d) show that the sample exhibits trigonal *P3m1* symmetry, with lattice parameters of $a = b = 8.22$ Å, $c = 10.03$ Å, and $\gamma = 120°$, which is consistent with previous reports.[9] The unit cell and crystal structure are illustrated in Figure 1 b and c. The structure shows metal halide octahedra layers, and the voids between the layers are filled with MA^+. One MA^+ group is surrounded by six metal halide octahedra. The PDF card was generated based on the atomic structure diagram (Table S2 in the Supporting Information).

The $MA_3Bi_2Br_9$ single crystal exhibits a PL peak at 550 nm and a FWHM of ca. 100 nm (Figure 1 e). There are two peaks in the PL spectrum, one peak at shorter wavelength (550 nm) which is attributed to band gap emission, and the shoulder peak at longer wavelength (580 nm) originating from bulk defects, similar to a previous report on $Cs_3Sb_2I_9$.[10] In addition, the PL peak exhibits a red shift relative to the transmission band edge. In order to determine the band gap, we used Tauc plot, which was obtained by tracing $(\alpha h\nu)^{1/r}$ versus $h\nu$, where α is the absorption coefficient. The parameter r denotes the type of transition, with a value of

[*] M. Y. Leng,[+] Z. W. Chen,[+] Y. Yang,[+] Dr. Z. Li, K. Zeng, K. H. Li, Dr. G. D. Niu, Y. S. He, Prof. J. Tang
Wuhan National Laboratory for Optoelectronics (WNLO) and School of Optical and Electronic Information
Huazhong University of Science and Technology
Wuhan, Hubei 430074 (China)
E-mail: guangda_niu@163.com
jtang@mail.hust.edu.cn

Q. C. Zhou
Beijing Key Laboratory of Nanophotonics and Ultrafine Optoelectronic Systems, School of Materials Science & Engineering
Beijing Institute of Technology
Haidian District, Beijing 100081 (China)

[+] These authors contributed equally to this work.

Supporting information for this article can be found under: http://dx.doi.org/10.1002/anie.201608160.

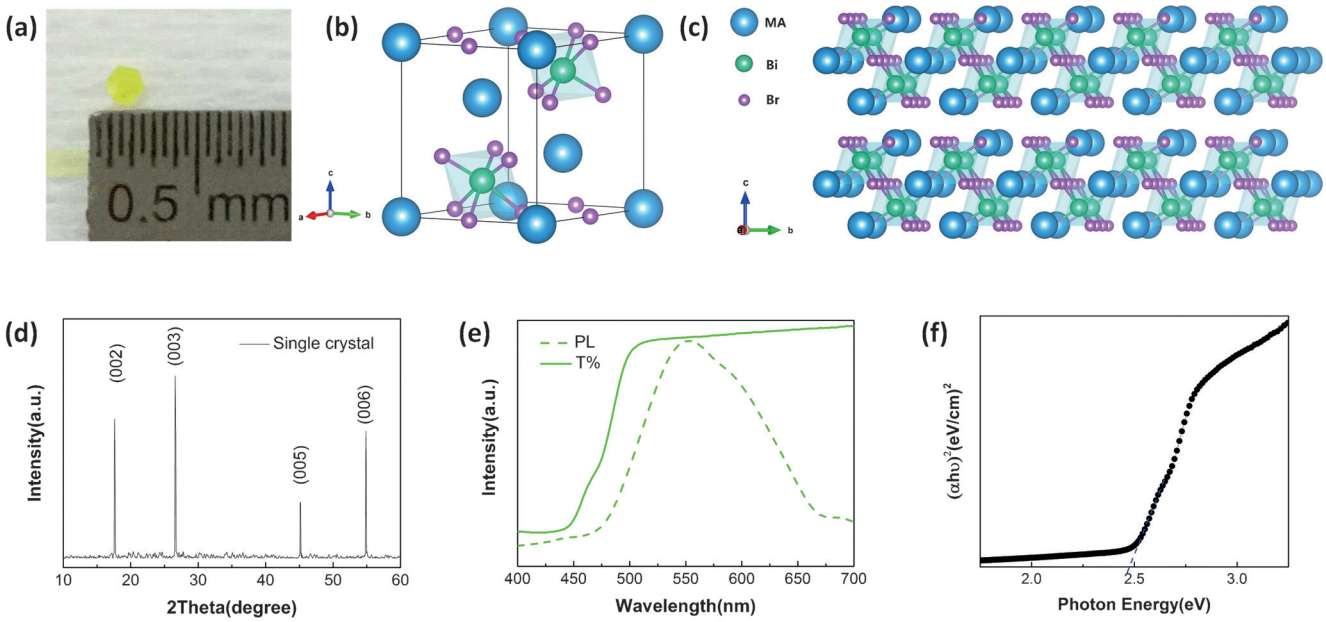

Figure 1. Properties of single-crystalline $MA_3Bi_2Br_9$. a) Photographs of perovskite single crystals. b) Unit cell. c) Crystal structure. d) Powder XRD spectra. e) Transmission (solid) and PL (dashed) spectra. f) Tauc plot ($n=2$; direct).

1/2 and 2 for direct and indirect band gaps, respectively. The fitting results indicate a direct band gap of 2.5 eV for $MA_3Bi_2Br_9$ single crystals (Figure 1 f).

For the synthesis of $MA_3Bi_2Br_9$ QDs, we used dimethylformamide (DMF) and ethyl acetate as the "good" solvents to dissolve MABr and $BiBr_3$. Octane acted as the "poor" solvent to precipitate QDs when the precursor solution was injected into octane. In addition, n-octylamine (OLAm) was dissolved into DMF to control the crystallization rate, and oleic acids (OA) was dissolved into octane to stabilize the colloidal solution. The typical synthesis process is shown in Figure S1a. Raman spectra for each step were recorded to follow the dissolution mechanism (Figure S1b).

Next, we optimized the synthesis process and found the highest PL intensity could be obtained with a precursor concentration of 0.2 mM, a MA/Bi ratio of 3:1, and a reaction temperature of 80 °C, as shown in Figure S2. Figure 2 b,c show photographs of colloidal solutions under sunlight and 365 nm illumination, respectively, indicating uniform QDs dispersed in the solvent without aggregation.

Typical transmission electron microscopy (TEM) images of $MA_3Bi_2Br_9$ QDs as well as the size distributions are presented in Figure 2 a and S1c. The synthesized $MA_3Bi_2Br_9$ QDs have an average diameter of 3.05 nm with a size deviation of ±0.9 nm. Figure 2 d shows the high-resolution transmission electron microscopy (HRTEM) image, with lattice distances of 3.56 and 3.34 Å corresponding to the (200) and (003) crystal facets, respectively. The corresponding fast Fourier transformation (FFT) image in the inset of Figure 2 d indicates the single-crystalline nature of the $MA_3Bi_2Br_9$ QD. Figure 2 e shows the XRD pattern of the as-synthesized QD powder (Figure S3), verifying the trigonal structure of $MA_3Bi_2Br_9$. In comparison with the single-crystal counterpart, the diffraction peaks are significantly broadened, which is caused by the limited size of colloidal QDs.

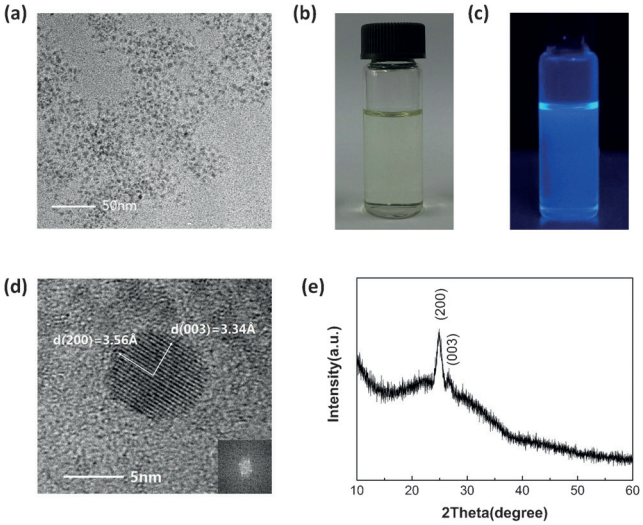

Figure 2. Properties of $MA_3Bi_2Br_9$ QDs. a) TEM image. b) Typical optical image of a colloidal $MA_3Bi_2Br_9$ solution. c) Colloidal $MA_3Bi_2Br_9$ solution under 365 nm UV light. d) HRTEM image of a typical QD. The inset in the bottom right corner is the corresponding FFT image. e) XRD patterns.

Since surface atoms play a vital role in determining the physical properties of QDs[11] and QDs usually have a non-stoichiometric atom ratio due to an either anion- or cation-rich surface, it was important to obtain surface information of the as-synthesized $MA_3Bi_2Br_9$ QDs. X-ray fluorescence (XRF) measurements show that the single crystal indeed has a Br/Bi ratio of 4.51 (Figure S4), which is consistent with the ideal atomic ratio of 4.5 according to chemical formula. XRF reveals that the as-synthesized $MA_3Bi_2Br_9$ QDs had a Br/Bi molar ratio of 5.12 (Figure 3 b), higher than the ideal stoichiometric ratio, implying a Br-rich QD surface. In order

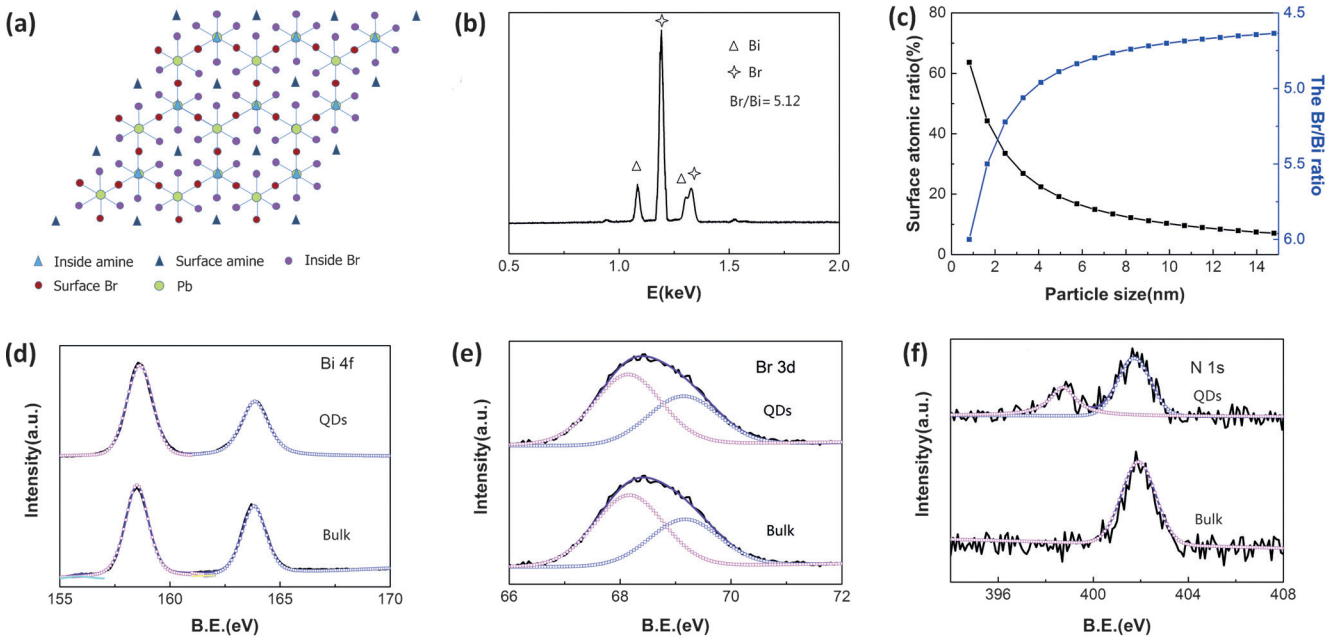

Figure 3. Characterization of $MA_3Bi_2Br_9$ QDs. a) Molecular structural model. b) XRF spectrum of a typical sample of $MA_3Bi_2Br_9$ QDs. c) Relationship between the percentage of surface atoms and the Br/Bi ratio with particle size. d–f) XPS spectra corresponding to Bi 4f (d), Br 3d (e), and N 1s (f) of $MA_3Bi_2Br_9$ QDs and bulk single crystals.

to further understand the specific composition of $MA_3Bi_2Br_9$ QDs, we established a simple model to correlate the particle size with the surface atomic ratio as well as Br/Bi atom ratio, assuming that the surface of QDs is terminated with Br atoms and amine groups (Figure 3a). Details of the model are shown in Table S4 and Figure S5. Based on this model we calculated a Br/Bi ratio for 3.05 nm $MA_3Bi_2Br_9$ QDs of 5.08 (Figure 3c), which is in good agreement with the Br/Bi ratio (5.12) from the XRF measurements.

X-ray photoelectron spectroscopy (XPS) measurements were used to investigate the surface composition of a single crystal and QDs, as shown in Figure 3d–f. Bi 4f and Br 3d spectra of $MA_3Bi_2Br_9$ QDs are in good agreement with that of bulk single crystals. The N 1s spectrum of $MA_3Bi_2Br_9$ QDs shows two peaks at 399.2 eV and 401.8 eV, which are attributed to $OLAm^+$ and MA^+, respectively. The $OLAm^+/(OLAm^+ + MA^+)$ ratio was calculated to be 38% based on the integral area of the two peaks. We also calculated the surface amine percentage for a 3.05 nm $MA_3Bi_2Br_9$ QD to be 44%, based on the model in Figure 3. From this results, it could be expected that $MA_3Bi_2Br_9$ QDs has a Bi-rich surface and most of the surface MA^+ is replaced by $OLAm^+$. Infrared spectra were recorded to study the surface ligands of $MA_3Bi_2Br_9$ QDs (Figure S6, Table S5). The peak at 657 cm^{-1} was attributed to Bi–O stretching, whereas the peaks at 1247 cm^{-1}, 1417 cm^{-1} and 1712 cm^{-1} were attributed to C–O stretching, O–H bending and C=O stretching from OA,[12] respectively, verifying the existence of bonding between surface Bi and OA.

We next studied the optical properties of $MA_3Bi_2Br_9$ QDs, as shown in Figure 4a. The absorption spectrum shows that the exciton peak of $MA_3Bi_2Br_9$ QDs is located around 376 nm. The PL spectrum exhibits an emission peak at

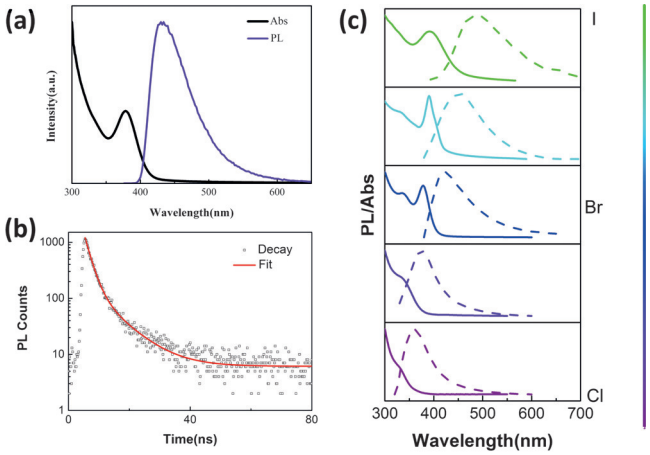

Figure 4. Optical properties of $MA_3Bi_2Br_9$ QDs. a) Absorption and PL spectra. b) Time-resolved PL decay and fitting curve of a typical sample. Composition-tunable absorption and PL spectra of perovskite $MA_3Bi_2X_9$ QDs by halide substitution.

423 nm with a FWHM of 62 nm. The sample showed a relative Stokes shift of 366 meV, implying almost no overlap between absorption and PL spectrum. Such a weak self-absorption is beneficial for the usage as phosphors in lighting application. Relative to the single crystal, the PL peak of QDs is blue-shifted by 120 nm, verifying a strong quantum confinement effect.

For the PLQY measurements with an integrating sphere, only a 378 nm laser was available as the excitation source. However, according to the excitation spectra, the fluorescence of $MA_3Bi_2Br_9$ QDs is almost negligible for excitation wavelengths longer than 370 mm (Figure S7). Thereby, we

applied a relative fluorescence test to obtain the PLQY value,[13] by using quinine sulfate acid aqueous solution as the standard sample (details in the Supporting Information). In order to verify the reliability of the method, we prepared $MAPbBr_3$ perovskite QDs with an emission peak at 450 nm. A PLQY of 63% was obtained by integrating sphere measurements, while 60% was obtained by relative fluorescence measurements. Next, we recorded the PLQYs of $MA_3Bi_2Br_9$ QDs ranging from 4% to 12% from different batches, which was comparable to all-inorganic Pb-based QDs with similar emission peaks ($CsPbCl_3$, emission peak: 405 nm, PLQY: 10%),[3f,h] but lower than for organic–inorganic layered perovskite with the formula of A_2PbBr_4 (A: $C_nH_{2n+1}NH_3$) in the same wavelength region ($\approx$22%).[14] This number represents a nearly 100-times improvement as compared to previous lead-free Sn-based perovskite QDs (best PLQY of 0.14%), suggesting Bi-based QDs are more promising as lead-free perovskite QDs.[7] Further improvement in PLQY of $MA_3Bi_2Br_9$ QDs may be achieved by either adopting new synthesis methods that would produce QDs with less defects, or by adding various ligands to passivate surface trap sites, such as didodecyldimethylammonium ion.[15]

Time-resolved PL spectra were used to reveal the exciton recombination dynamics, as shown in Figure 4b. The PL decay could be fitted by a biexponential function, giving a short-lived PL lifetime (τ1) of 1.96 ns with a percentage of 98% and long-lived PL lifetime (τ2) of 7.99 ns with a percentage of 2%. According to previous studies, the short-lived lifetime can be attributed to exciton recombination while the long-lived component might correlate to surface defect recombination.[16] Therefore, the fluorescence decay of $MA_3Bi_2Br_9$ QDs proceeds predominantly by exciton radiative recombination.

Colloidal $MA_3Bi_2X_9$ QDs, where X represents mixed halide compositions, were prepared through post-synthetic anion exchange.[17] Figure S8 shows the photographs and PL spectra of the synthesized samples. As shown in Figure 4c, the absorption and PL spectra can be fine-tuned by varying the anion composition (Br, Cl, and I), with PL peaks ranging from 360 to 540 nm. When Br atoms were partially replaced with Cl or I, the band gaps increased or decreased, respectively, leading to composition-dependent photoluminescence. PLQY and emission peaks of such anion-exchanged QDs are summarized in Table 1.

Finally, we studied the stability of $MA_3Bi_2Br_9$ QDs. Unexpectedly, $MA_3Bi_2Br_9$ QDs exhibited superior stability toward ethanol compared to $MAPbBr_3$ QDs. After adding 0.1 mL ethanol to 5 mL $MAPbBr_3$ QDs solution, the fluorescence was rapidly quenched, whereas the $MA_3Bi_2Br_9$ QDs showed almost no fluorescence change upon the same treatment (Figure S9). The high stability of $MA_3Bi_2Br_9$ QDs in ethanol could be beneficial for fabricating the top organic electron (hole) transport layers for application in light emitting diodes. However, the moisture stability was still not satisfactory. It was observed that $BiCl_3$ easily reacted with water to generate BiOCl (Table S6), so did $BiBr_3$. We placed $MA_3Bi_2Br_9$ powder, which was obtained by grinding of the single crystal, in water. The powder turned into white BiOBr in seconds (Figure S10). Similarly, for the colloidal QDs solution, white powders also precipitated out after one-week storage in humid environment (24 °C, relative humidity of 80%).

The photostability of $MA_3Bi_2Br_9$ QDs solutions was also studied (Figure S11). The solutions were illuminated with a portable UV lamp (254 nm, 6 W, 1 cm distance) and exhibited a gradual decrease in PL intensity, as it was similarly observed for Pb-based perovskite and CdSe QDs.[18] It was reported that surface defects caused by oxygen exposure are responsible for the decomposition of perovskite QDs and PL degradation. When 1 sun illumination was applied instead of UV light, the $MA_3Bi_2Br_9$ QDs showed higher stability, with only 8% decrease of PL intensity after 1500 min illumination (Figure S12).

In summary, we prepared single-crystalline $MA_3Bi_2Br_9$ perovskite and determined its crystal structure and fundamental material properties. The $MA_3Bi_2Br_9$ perovskite QDs exhibited PLQYs up to 12%, which is comparable to all-inorganic Pb-based QDs. The PL emission peaks of $MA_3Bi_2Br_9$ QDs can be easily tuned from 360 to 540 nm by controlling the anion composition. Bismuth-based QDs are new members to the family of hybrid perovskite QDs and show great potential for light emitting diodes owing to their (presumed) low toxicity, favorable PLQY in the blue/violet spectral region, good ethanolic stability and insignificant re-absorption effect.

Table 1: Summary of PLQY and emission peaks for colloidal $MA_3Bi_2X_9$ QDs with different halide compositions.

QDs	PLQY [%]	Emission peak [nm]	FWHM [nm]
$MA_3Bi_2Cl_9$	15	360	50
$MA_3Bi_2Br_9$	12	423	62
$MA_3Bi_2I_9$	0.03	540	91

Acknowledgements

This work was supported by the National Natural Science Foundation of China (NO. 61274055), the National Key Research and Development Program of China (2016YFA0204000 and 2016YFB0700700), the Director Fund of WNLO, the Self-determined Innovative Research Funds for the Central Universities, HUST (2016JCTD111), and the State Key Laboratory of Luminescence and Applications (SKLA-2016-08). We thank Prof. H. Zhong at the Beijing Institute of Technology for helpful discussions and Prof. L. Xu at WNLO for providing access to PL facilities.

Keywords: bismuth · $MA_3Bi_2Br_9$ · perovskites · photoluminescence · quantum dots

How to cite: *Angew. Chem. Int. Ed.* **2016**, *55*, 15012–15016
Angew. Chem. **2016**, *128*, 15236–15240

[1] Y. Shirasaki, G. J. Supran, M. G. Bawendi, V. Bulović, *Nat. Photonics* **2012**, *7*, 13.
[2] B. T. Diroll, C. B. Murray, *ACS Nano* **2014**, *8*, 6466.

[3] a) H. Huang, F. Zhao, L. Liu, F. Zhang, X. Wu, L. Shi, B. Zou, Q. Pei, H. Zhong, *ACS Appl. Mater. Interfaces* **2015**, *7*, 28128; b) Y. Zhao, K. Zhu, *Chem. Soc. Rev.* **2016**, *45*, 655; c) S. T. Ha, X. Liu, Q. Zhang, D. Giovanni, T. C. Sum, Q. Xiong, *Adv. Opt. Mater.* **2014**, *2*, 838; d) S. Gonzalez-Carrero, R. E. Galian, J. Pérez-Prieto, *J. Mater. Chem. A* **2015**, *3*, 9187; e) A. Kojima, M. Ikegami, K. Teshima, T. Miyasaka, *Chem. Lett.* **2012**, *41*, 397; f) L. Protesescu, S. Yakunin, M. I. Bodnarchuk, F. Krieg, R. Caputo, C. H. Hendon, R. X. Yang, A. Walsh, M. V. Kovalenko, *Nano Lett.* **2015**, *15*, 3692; g) J. Song, J. Li, X. Li, L. Xu, Y. Dong, H. Zeng, *Adv. Mater.* **2015**, *27*, 7162; h) X. Li, Y. Wu, S. Zhang, B. Cai, Y. Gu, J. Song, H. Zeng, *Adv. Funct. Mater.* **2016**, *26*, 2435; i) Y. Wang, X. Li, J. Song, L. Xiao, H. Zeng, H. Sun, *Adv. Mater.* **2015**, *27*, 7101; j) D. Zhang, S. W. Eaton, Y. Yu, L. Dou, P. Yang, *J. Am. Chem. Soc.* **2015**, *137*, 9230; k) Q. A. Akkerman, V. D. Innocenzo, S. Accornero, A. Scarpellini, A. Petrozza, M. Prato, L. Manna, *J. Am. Chem. Soc.* **2015**, *137*, 10276; l) A. B. Wong, M. Lai, S. W. Eaton, Y. Yu, E. Lin, L. Dou, A. Fu, P. Yang, *Nano Lett.* **2015**, *15*, 5519.

[4] a) D. N. Dirin, S. Dreyfuss, M. I. Bodnarchuk, G. Nedelcu, P. Papagiorgis, G. Itskos, M. V. Kovalenko, *J. Am. Chem. Soc.* **2014**, *136*, 6550; b) X. Gong, Z. Yang, G. Walters, R. Comin, Z. Ning, E. Beauregard, V. Adinolfi, O. Voznyy, E. H. Sargent, *Nat. Photonics* **2016**, *10*, 253; c) J. Xing, F. Yan, Y. Zhao, S. Chen, H. Yu, Q. Zhang, R. Zeng, H. V. Demir, X. Sun, A. Huan, Q. Xiong, *ACS Nano* **2016**, *10*, 6623; d) W. Zhang, G. E. Eperon, H. J. Snaith, *Nat. Energy* **2016**, *1*, 16048; e) X. Zhang, H. Lin, H. Huang, C. Reckmeier, Y. Zhang, W. C. H. Choy, A. L. Rogach, *Nano Lett.* **2016**, *16*, 1415.

[5] a) A. H. Slavney, T. Hu, A. M. Lindenberg, H. I. Karunadasa, *J. Am. Chem. Soc.* **2016**, *138*, 2138; b) S. Sun, S. Tominaka, J. Lee, F. Xie, P. D. Bristowe, A. K. Cheetham, *APL Mater.* **2016**, *4*, 031101; c) I. P. Aleksandrova, R. Burriel, J. Bartolome, B. S. Bagautdinov, J. Blasco, A. A. Sukhovsky, J. M. Torres, A. D. Vasiljev, L. A. Solovjev, *Phase Transitions* **2002**, *75*, 607.

[6] T. C. Jellicoe, J. M. Richter, H. F. J. Glass, M. Tabachnyk, R. Brady, S. E. Dutton, A. Rao, R. H. Friend, D. Credgington, N. C. Greenham, M. L. Böhm, *J. Am. Chem. Soc.* **2016**, *138*, 2941.

[7] B. Park, B. Philippe, X. Zhang, H. Rensmo, G. Boschloo, E. M. J. Johansson, *Adv. Mater.* **2015**, *27*, 6806.

[8] F. Zhang, H. Zhong, C. Chen, X. Wu, X. Hu, H. Huang, J. Han, B. Zou, Y. Dong, *ACS Nano* **2015**, *9*, 4533.

[9] M. Iwata, Y. Ishibashi, *Ferroelectrics* **1992**, *135*, 283.

[10] B. Saparov, F. Hong, J. Sun, H. Duan, W. Meng, S. Cameron, I. G. Hill, Y. Yan, D. B. Mitzi, *Chem. Mater.* **2015**, *27*, 5622.

[11] M. A. Boles, D. Ling, T. Hyeon, D. V. Talapin, *Nat. Mater.* **2016**, *15*, 141.

[12] S. S. Pati, L. H. Singh, E. M. Guimarães, J. Mantilla, J. A. H. Coaquira, A. C. Oliveira, V. K. Sharma, V. K. Garg, *J. Alloys Compd.* **2016**, *684*, 68.

[13] A. T. R. Williams, S. A. Winfield, N. M. James, *Analyst* **1983**, *108*, 1067.

[14] a) S. Gonzalez-Carrero, G. M. Espallargas, R. E. Galian, J. Pérez-Prieto, *J. Mater. Chem. A* **2015**, *3*, 14039; b) N. Kawano, M. Koshimizu, Y. Sun, N. Yahaba, Y. Fujimoto, T. Yanagida, K. Asai, *J. Phys. Chem. C* **2014**, *118*, 9101.

[15] J. Pan, S. P. Sarmah, B. Murali, I. Dursun, W. Peng, M. R. Parida, J. Liu, L. Sinatra, N. Alyami, C. Zhao, E. Alarousu, T. K. Ng, B. S. Ooi, O. M. Bakr, O. F. Mohammed, *J. Phys. Chem. Lett.* **2015**, *6*, 5027.

[16] G. D. Scholes, G. Rumbles, *Nat. Mater.* **2006**, *5*, 683 – 696.

[17] D. M. Jang, K. Park, D. H. Kim, J. Park, F. Shojaei, H. S. Kang, J. Ahn, J. W. Lee, J. K. Song, *Nano Lett.* **2015**, *15*, 5191.

[18] a) H. Peng, L. Zhang, C. Soeller, J. Travas-Sejdic, *J. Lumin.* **2007**, *127*, 721; b) H. Wang, S. Lin, A. Tang, B. P. Singh, H. Tong, C. Chen, Y. Lee, T. Tsai, R. Liu, *Angew. Chem. Int. Ed.* **2016**, *55*, 7924; *Angew. Chem.* **2016**, *128*, 8056; c) Y. He, H. Lu, L. Sai, Y. Su, M. Hu, C. Fan, W. Huang, L. Wang, *Adv. Mater.* **2008**, *20*, 3416; d) O. Chen, J. Zhao, V. P. Chauhan, J. Cui, C. Wong, D. K. Harris, H. Wei, H. S. Han, D. Fukumura, R. K. Jain, M. G. Bawendi, *Nat. Mater.* **2013**, *12*, 445 – 451.

Received: August 20, 2016
Revised: September 25, 2016
Published online: October 28, 2016

